Charge-carrier dynamics of solution-processed antimony- and bismuth-based chalcogenide thin films

Zhenglin Jia[1,2,#], Marcello Righetto[3,#], Yujie Yang[1,2], Chelsea Q. Xia[3], Yanyan Li[1,2], Ruiming Li[1,2], Yuwei Li[1,2], Bin Yu[1,2], Yong Liu[1], Huiming Huang[1], Michael B. Johnston[3], Laura M. Herz[3,4,] and Qianqian Lin[1,2,*]*

[1]Key Lab of Artificial Micro- and Nano-Structures of Ministry of Education of China, School of Physics and Technology, Wuhan University, Wuhan, Hubei, 430072, P. R. China

[2] Hubei Luojia Laboratory, Wuhan, Hubei, 430072, P. R. China.

[3] Department of Physics, University of Oxford, Clarendon Laboratory, Parks Road, Oxford, OX1 3PU, U.K.

[4] Institute for Advanced Study, Technical University of Munich, Lichtenbergstrasse 2a, 85748, Garching, Germany.

[#] These authors contributed equally: Zhenglin Jia and Marcello Righetto

[*]Correspondence: Laura.Herz@physics.ox.ac.uk (L.M.H.), q.lin@whu.edu.cn (Q.L.)

1. EXPERIMENTAL SECTION

1.1 Chemicals and reagents

Antimony acetate ($Sb(Ac)_3$, 99.99%) was purchased from Sigma Aldrich. Thiourea (TU, 99%) was purchased from Alfa Aesar. Silver nitrate ($AgNO_3$, 99.8%) was purchased from Chengdu Chron Chemicals. Bismuth nitrate pentahydrate ($Bi(NO_3)_3 \cdot 5H_2O$, 98.0%) was purchased from Sigma Aldrich. 2-Methoxyethanol (2-Me, 99%) and dimethyl sulfoxide (DMSO, 99.9%) were purchased from Aladdin. All commercial products were used as received.

1.2 Fabrication of chalcogenide thin films via solution process

1.2.1 Sb_2S_3 thin films

Sb_2S_3 precursor was prepared with sol-gel method. Firstly, 35 μL deionized water was added into 800 μL DMSO and mixed for 12 h. Then, 500 mg $Sb(Ac)_3$ was added into the mixed solvent and stirred for 10 h at room temperature. Finally, 250 mg TU was added in the solution and stirred for another 5 h at room temperature. Then, Sb_2S_3 films were deposited on the substrates by spin-coating at 4000 RPM for 60 s, and followed by a low temperature pre-annealing on a hot plate at 220 °C for 1 min and a high temperature annealing at 320 °C for 10 min in glovebox with nitrogen atmosphere.

1.2.2 $AgSbS_2$ thin films

$AgSbS_2$ precursor was prepared by dissolving 169.87 mg $AgNO_3$ in the mixed solvent of 1 mL DMSO and 10 μL deionized water. Then, 197.86 mg TU was added in the solution. After that, 298.892 mg $Sb(Ac)_3$ was added in the above solution. The solution was then stirred at room temperature for 3 h to from the final precursor. Subsequently, $AgSbS_2$ films were deposited on

the substrates by spin-coating at 7000 RPM for 40 s, and pre-annealed at 120 °C for 2 min and further annealed at 350 °C for 5 min in glovebox with nitrogen atmosphere.

1.2.3 Bi_2S_3 thin films

Bi_2S_3 precursor was prepared by adding 121.25 mg $Bi(NO_3)_3 \cdot 5H_2O$ into 500 μL 2-Me and stirring until fully dissolved. Then, 38.06 mg TU was added into the solution and stirred until fully dissolved. By adding different amounts of TU, we can obtain solutions with different Bi-S ratios. Then, the Bi_2S_3 films were obtained by spin-coating the precursor solution on the substrates at 2500 RPM for 50 s, followed by a low temperature pre-annealing on a hot plate at 100 °C for 10 min and a high temperature annealing on a hot plate at 280 °C for 15 min in glovebox with nitrogen atmosphere.

1.2.4 $AgBiS_2$ thin films

$AgBiS_2$ precursor was prepared by dissolving 101.92 mg $AgNO_3$, 291 mg $Bi(NO)_3 \cdot 5H_2O$ and 91.34 mg TU into 1mL DMSO and stirring until fully dissolved at room temperature. The $AgBiS_2$ films were obtained by spin-coating the solution on the substrates at 3000 RPM for 60 s. Then, the $AgBiS_2$ films were annealed for 30 min at 100 ° C, 150 ° C, 200 ° C and 300 ° C respectively. All the above procedures were carried out in the glovebox with nitrogen atmosphere.

1.3 Fabrication of chalcogenide based photoconductors

Indium tin oxide (ITO)-coated glass was patterned with 100 μm channels by a high power (80 W) 1064 nm nanosecond pulse laser. Then, ITO -coated glass was sprayed with detergent and gently brushed clean with a toothbrush, followed by sonication, in turn, with deionized water and ethanol for 15 min each. The substrates were dried with an air-gun and treated with UV-ozone

before depositing thin films. Finally, various chalcogenide films were deposited by spin-coating of precursors.

1.4 Characterisation

The surface morphology of various chalcogenide films was obtained with a Zeiss GeminiSEM 500 Field Emission Scanning Electron Microscope System. The thickness and roughness of the obtained chalcogenide films was measured by a step profiler (Alpha-Step D-500). The crystal structure was characterized with X-ray diffraction (XRD) using a D8 Advance X-ray diffractometer (Cu Kα = 1.5418 Å) with a scanning range from 10 to 50°. The absorption spectra were tested with an ultraviolet spectrophotometer (PerkinElmer LAMBDA 1050). Photoluminescence spectra were recorded with a fiber optic spectrometer (Ideaoptics, NOVA-EX), and the samples were placed in a cryostat (Janis, 20 K-300 K), and excited with a CW 405 nm laser with an intensity of 0.5 W cm^{-2}. The photoconductivity of various sulfide films was tested at room temperature with a semiconductor analyzer (Keysight, B1500A) under the illumination of LED with a wavelength of 530 nm (Thorlabs). The temperature-dependent photoconductivity was also measured by a semiconductor analyzer (Keysight, B1500A) and the temperature was modulated with a cryostat (Instec, LN2-P4C, C100W) under vacuum.

2. SUPPLEMENTARY NOTES

2.1 **Supplementary Note 1: TRMC measurements**

The time-resolved microwave conductivity (TRMC) measurement is an electrode-free technique, which can probe the charge carrier dynamics of semiconductors.[1, 2] The samples were excited with a fast laser pulse (~5 ns), which generate a certain amount of carriers within the semiconductor thin films, which can absorb the microwave. Then, we monitor transmittance or

reflectance of the microwave as a function of time after the photoexcitation, the decay curves can be obtained. To enhance to absorption of microwaves and recorded signal, we introduce a high-Q microwave cavity, which has the resonance frequency at ~ 4.3 GHz. The source power of the microwave was set to be 1 mW, and the excitation laser wavelength is tunable (200 nm ~2400 nm) with a pulse fluence of ~1-100 μJ cm^{-2}. The change of the microwave conductivity of the samples can be correlated with the change of detected microwave power by a sensitivity factor (K) as follows,

$$\frac{\Delta P(\mathrm{t})}{P} = -k\Delta G(\mathrm{t}) \ , \qquad (1)$$

where $\Delta P(t)/P$ is the change of the detected microwave power and $\Delta G(t)$ is the change of the conductance. The geometrical dimensions of the samples and the dielectric properties of the media in the microwave cavity mainly determine the sensitivity factor. Based on the maximum change of the conductance and the incident light intensity (I_0), we can determine the mixed mobility ($\sum\mu$) as follows,

$$\varphi\Sigma\mu = \frac{\Delta G_{\max}}{I_0\beta_{TRMC}eF_A} \ , \qquad (2)$$

Where φ is the charge carrier generation yield, β_{TRMC} is the ratio between the broad and narrow inner dimensions of the waveguide, e is the elementary charge and F_{A} is the optical attenuation.

2.2 **Supplementary Note 2: OPTP measurements**

Optical-pump-terahertz-probe (OPTP) spectroscopy is a noncontact probe for AC conductivity at THz frequencies and can be used to extract the charge-carrier mobility of the material. To perform OPTP experiments, we used a setup described in more detail elsewhere.[3] The setup uses the 1.55 eV fundamental output (35-fs pulse duration, 5-kHz repetition rate) of an amplified Ti:sapphire laser (Spectra-Physics Spitfire). We use a fraction of this output to generate THz pulses in a spintronic emitter via the inverse spin Hall effect. In the setup, samples are excited by frequency-doubled 3.1 eV pulses obtained by second-harmonic generation in a beta-barium-borate (BBO) crystal. We then monitor fractional changes in the THz transmittance by using free-space electro-optic (EO) sampling. Here, the THz detection setup uses a 1 mm-thick ZnTe (110) crystal, a Wollaston prism and a balanced photodiodes pair. All the measured samples are thin film samples deposited onto z-cut quartz (2 mm). We perform OPTP measurements under vacuum (samples, THz generation and detection) at pressures 5×10^{-2} mbar.

We extracted THz charge-carrier mobilities from the OPTP data by converting the initial change in photoinduced transmission of THz radiation through a thin-film optical model, following the approach developed by Wehrenfennig *et al.*.[4] Here, we converted the fractional change in THz transmission $-\Delta T/T$ traces to sheet photoconductivity traces ΔS. Considering our experimental geometry (*i.e.*, transmission measurement through a thin film with a thickness much smaller than the THz wavelength), we can approximate the measured sheet photoconductivity to

$$\Delta S = -\epsilon_0 c(n_{quartz} + n_{vacuum})\left(\frac{\Delta T}{T}\right) \quad , \quad (3)$$

where $n_{\text{quartz}} = 2.13$ and $n_{\text{vacuum}} = 1$ are the refractive indexes of quartz and vacuum, respectively. To extract the charge-carrier mobility from the initial photoconductivity values, we determined the photogenerated carrier density following the pump excitation. This will be proportional to the number of absorbed photons N, defined as

$$N = \phi \frac{E\lambda}{hc}\left(1 - R_{pump} - T_{pump}\right) \quad , \quad (4)$$

where ϕ, E, and $\varepsilon = hc/\lambda$ are the photon-to-charge branching ratio (*i.e.*, the fraction of generated charges per photons absorbed), the excitation energy per pulse, and the energy of a photon with wavelength λ, respectively. Furthermore, R and T are the sample transmittance and reflectance at the pump energy, determined by reflection-transmission experiments. The resulting charge carrier mobility is given by

$$\mu = \frac{\Delta S A_{eff}}{Ne} \quad , \quad (5)$$

where A_{eff} is the effective overlap area between THz and pump beam and e the elementary charge. Combining Eq. 5 with Eq.3 and Eq.4 yields an expression for the resulting charge carrier mobility. However, since ϕ is generally unknown, the quantity derived from the OPTP experiments is the effective mobility $\tilde{\mu} = \phi\mu$, described as

$$\phi\mu = -\epsilon_0 c(n_{quartz} + n_{vacuum}) \frac{A_{eff} hc}{eE\lambda(1-R-T)}\left(\frac{\Delta T}{T}\right) \quad . \quad (6)$$

2.3 **Supplementary Note 3: calculation of absorption coefficients**

The thin film absorption was severely affected by interference effects. Hence, we recorded both transmittance and reflectance spectra of these chalcogenide thin films. Hence, the absorption coefficient (α) could be determined by the reflectance (R) corrected transmittance (T) spectra, given by,

$$T = (1 - R)e^{-\alpha d} \quad , \qquad (7)$$

where d is the film thickness. We can also obtain the real absorbance of these samples according to,

$$Abs = \log(\frac{1-R}{T}) \quad . \qquad (8)$$

3. SUPPORTING FIGURES

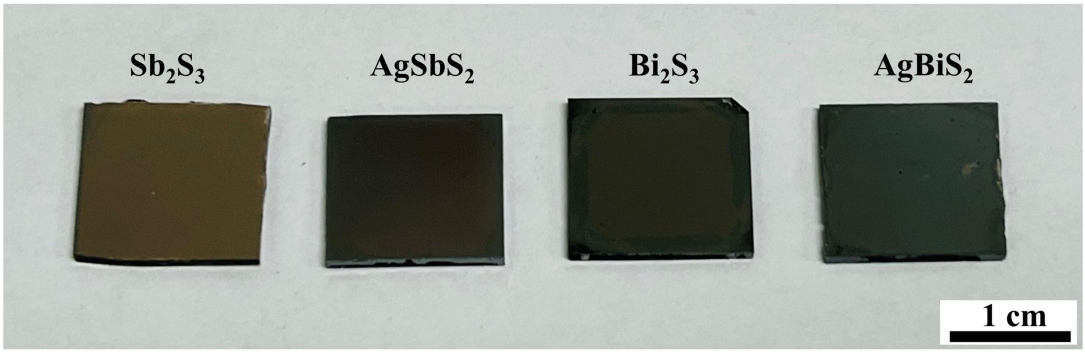

Figure S1. Optical photos of solution-processed Sb_2S_3, $AgSbS_2$, Bi_2S_3 and $AgBiS_2$ thin films.

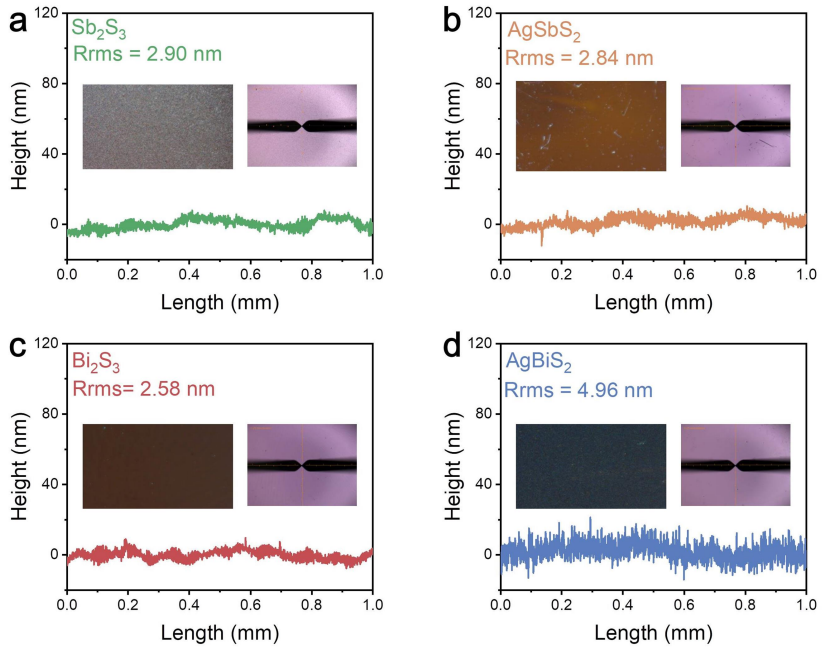

Figure S2. Surface roughness scan of the chalcogenide thin films, (**a**) Sb_2S_3, (**b**) $AgSbS_2$, (**c**) Bi_2S_3 and (**d**) $AgBiS_2$.

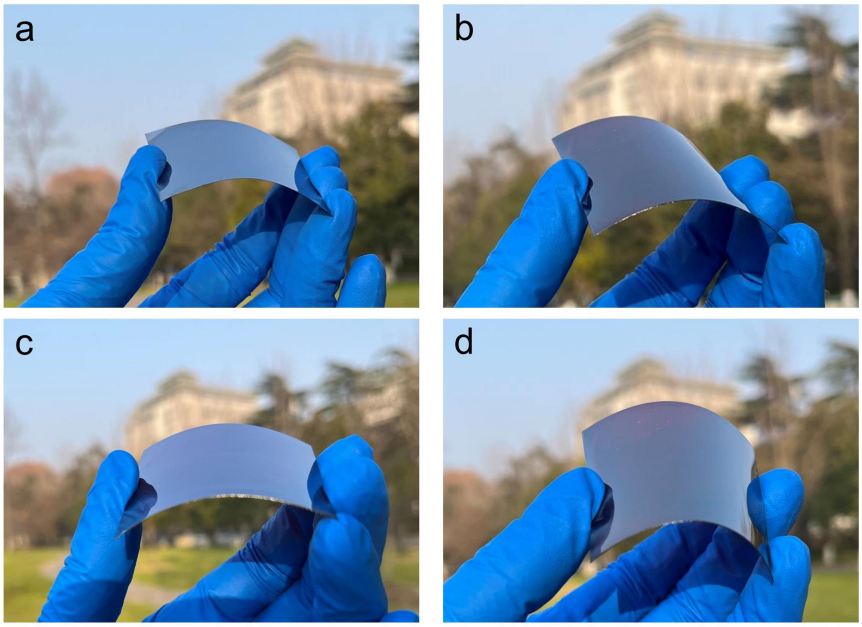

Figure S3. Optical photos of chalcogenide thin films, (**a**) Sb_2S_3, (**b**) $AgSbS_2$, (**c**) Bi_2S_3 and (**d**) $AgBiS_2$ deposited on large area (5 cm× 5 cm) flexible substrates.

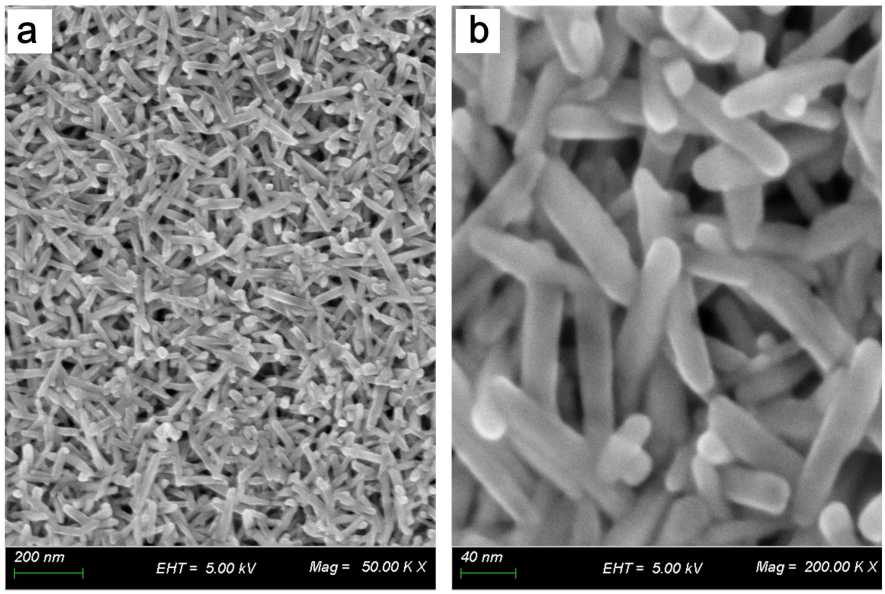

Figure S4. SEM images of Bi_2S_3 with different magnifications, (**a**) 50 k and (**b**) 200 k.

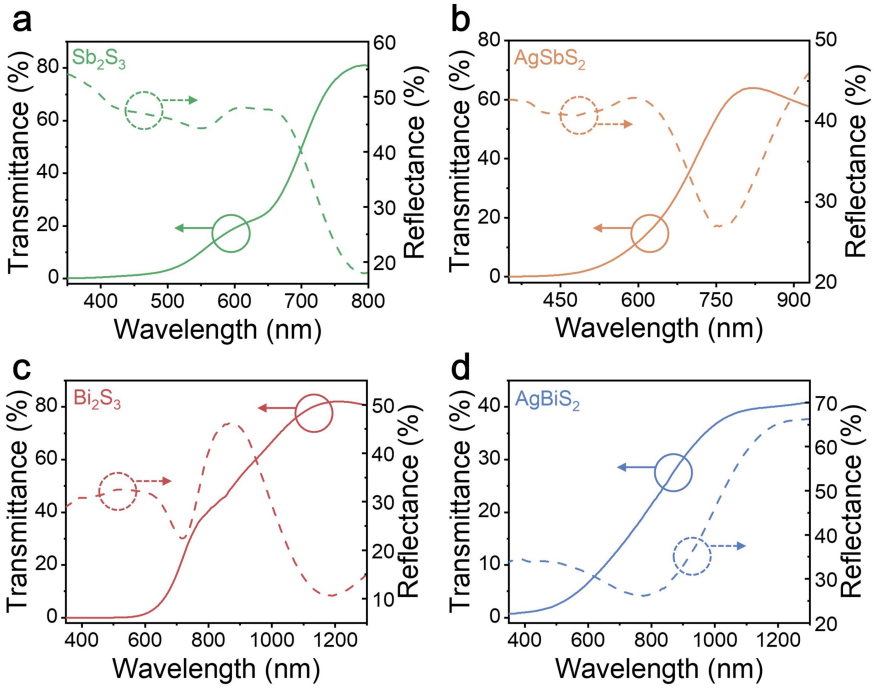

Figure S5. Transmittance and reflectance spectra of (**a**) Sb_2S_3, (**b**) $AgSbS_2$, (**c**) Bi_2S_3 and (**d**) $AgBiS_2$ thin films.

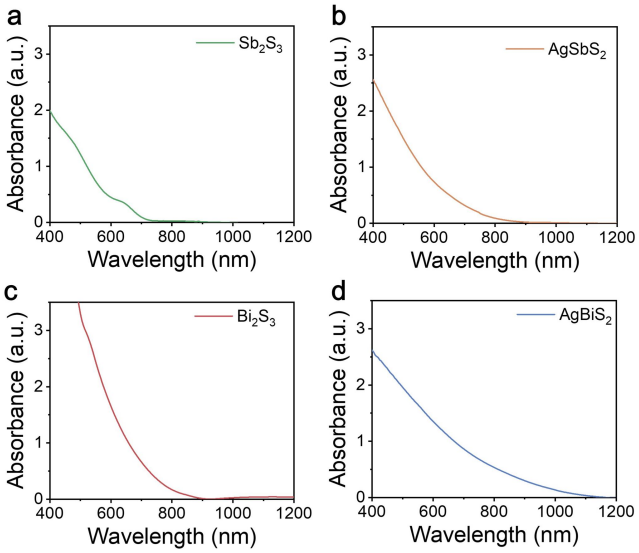

Figure S6. Absorption spectra of (**a**) Sb_2S_3 (110 nm), (**b**) $AgSbS_2$ (135 nm), (**c**) Bi_2S_3 (155 nm) and (**d**) $AgBiS_2$ (100 nm) thin films.

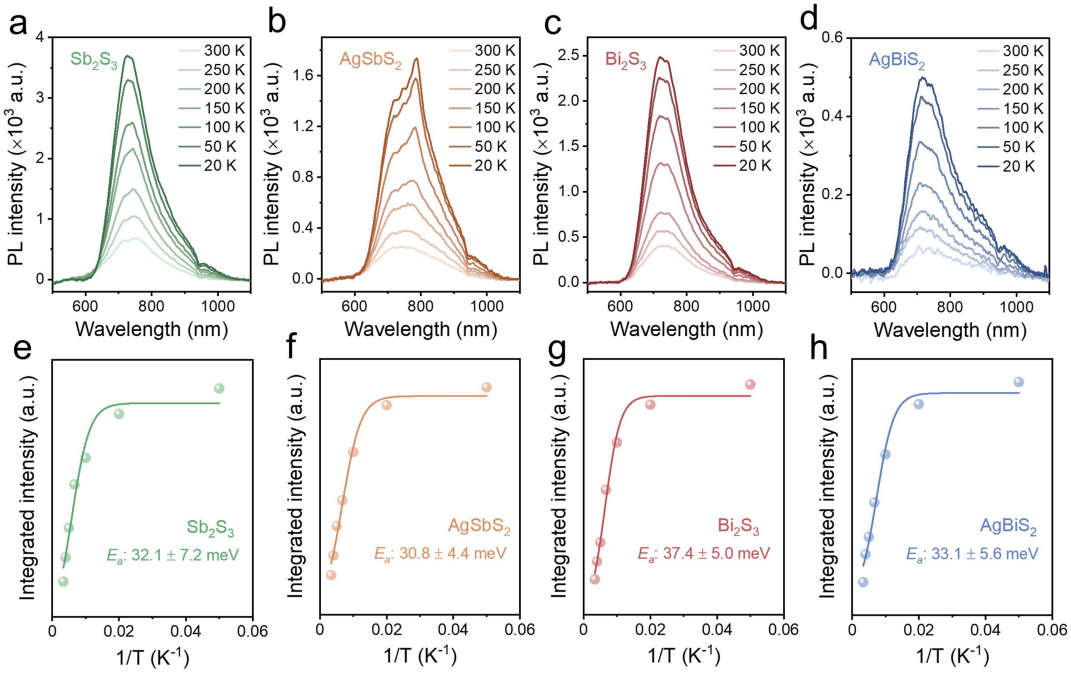

Figure S7. Comparison of the temperature-dependent photoluminescence spectra of the solution-processed (**a**) Sb_2S_3 (**b**) $AgSbS_2$, (**c**) Bi_2S_3 and (**d**) $AgBiS_2$ thin films, and the extracted activation energy by fitting the temperature dependent-integrated PL intensity of (**e**) Sb_2S_3, (**f**) $AgSbS_2$, (**g**) Bi_2S_3 and (**h**) $AgBiS_2$.

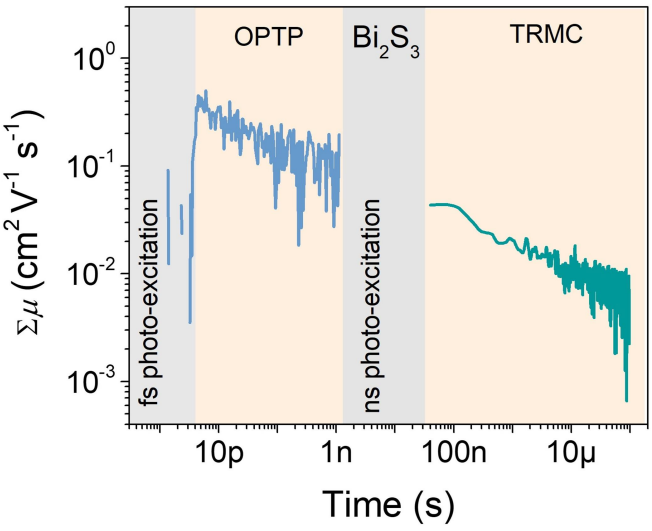

Figure S8. OPTP decay plotted with the TRMC decay of Bi_2S_3 samples under excitation fluence of ~70 μJ cm^{-2}.

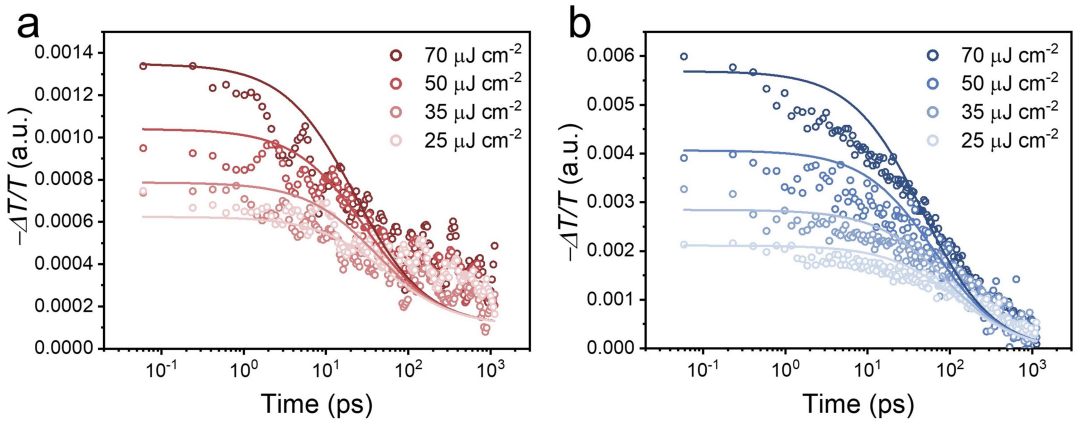

Figure S9. Fitting of fluence dependent of OPTP traces of (**a**) Bi_2S_3 and (**b**) $AgBiS_2$ samples.

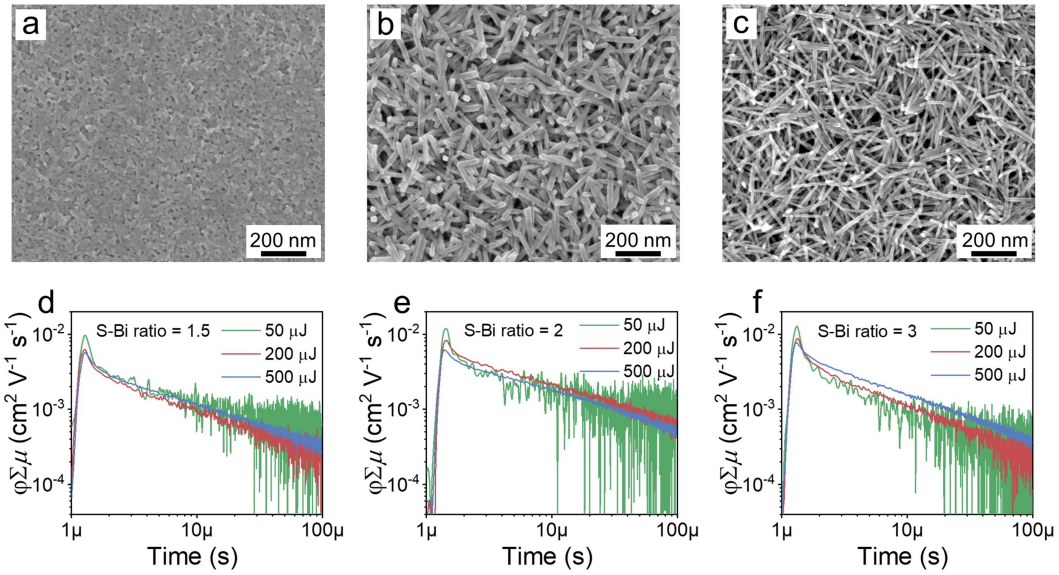

Figure S10. Comparison of the SEM images of Bi_2S_3 nanorods prepared with S-Bi ratio of (**a**) 1.5, (**b**) 2 and (**c**) 3, and fluence dependent TRMC decays of Bi_2S_3 nanorods prepared with S-Bi ratio of (**d**) 1.5, (**e**) 2 and (**f**) 3.

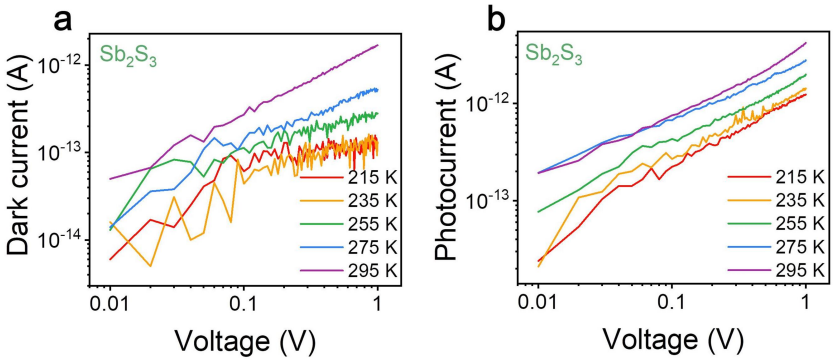

Figure S11. Temperature dependent **(a)** dark and (**b**) photoconductivity of Sb_2S_3 thin films.

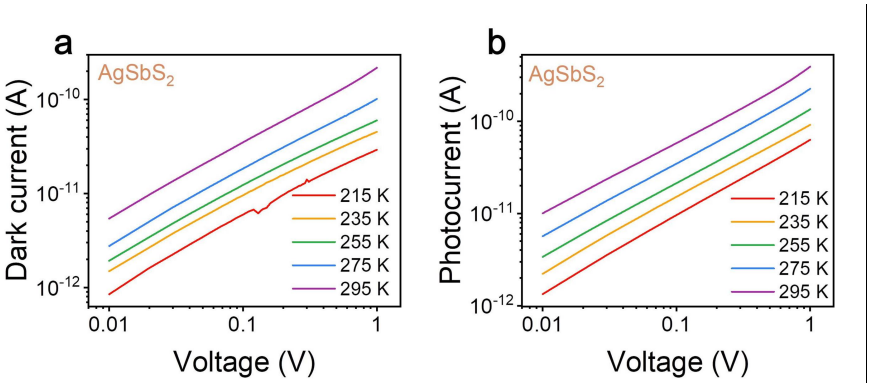

Figure S12. Temperature dependent **(a)** dark and (**b**) photoconductivity of $AgSbS_2$ thin films.

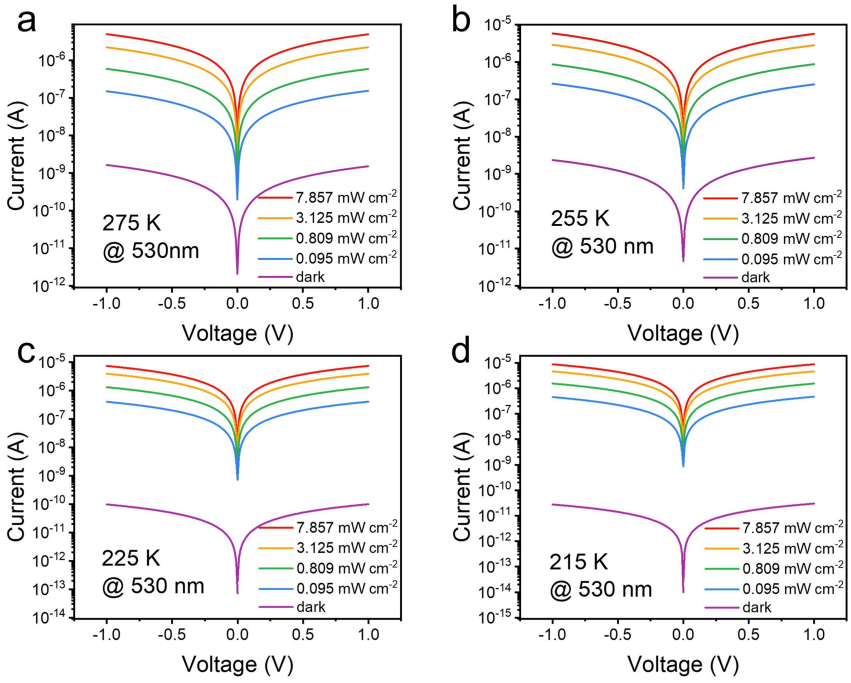

Figure S13. Light intensity dependent *I-V* curves of Bi_2S_3 photoconductors at (**a**) 275 K, (**b**) 255 K, (**c**) 225 K and (**d**) 215 K, respectively.

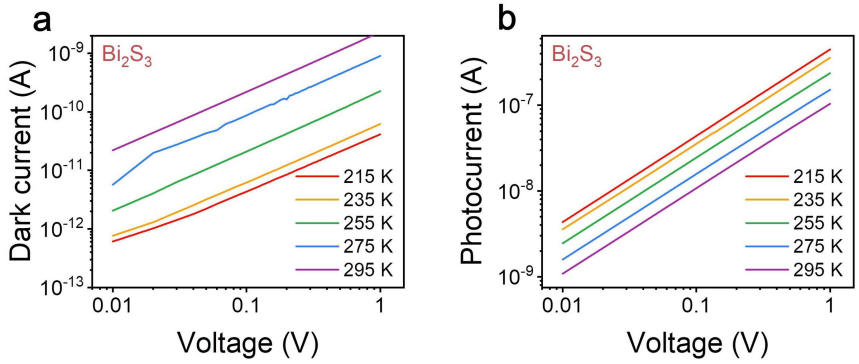

Figure S14. Temperature dependent **(a)** dark and (**b**) photoconductivity of Bi_2S_3 thin films.

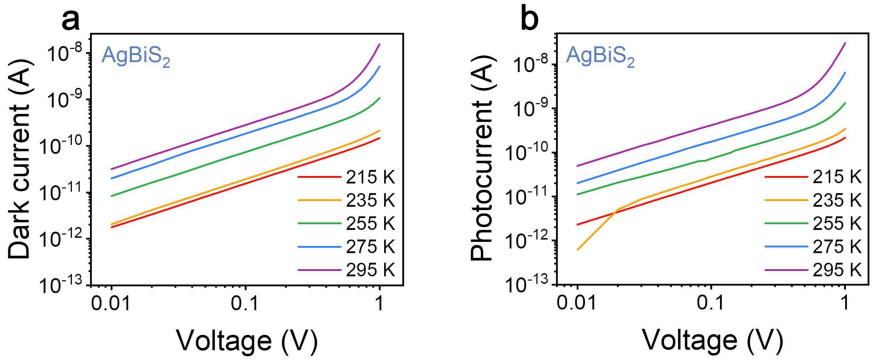

Figure S15. Temperature dependent **(a)** dark and (**b**) photoconductivity of $AgBiS_2$ thin films.

References

(1) Chattopadhyay, S.; Kokenyesi, R. S.; Hong, M. J.; Watts, C. L.; Labram, J. G. Resolving in-plane and out-of-plane mobility using time resolved microwave conductivity. ***J. Mater. Chem. C*** **2020**, *8* (31), 10761.

(2) Ponseca, C. S., Jr.; Savenije, T. J.; Abdellah, M.; Zheng, K.; Yartsev, A.; Pascher, T.; Harlang, T.; Chabera, P.; Pullerits, T.; Stepanov, A.; et al. Organometal halide perovskite solar cell materials rationalized: ultrafast charge generation, high and microsecond-long balanced mobilities, and slow recombination. ***J. Am. Chem. Soc.*** **2014**, *136* (14), 5189.

(3) Buizza, L. R.; Wright, A. D.; Longo, G.; Sansom, H. C.; Xia, C. Q.; Rosseinsky, M. J.; Johnston, M. B.; Snaith, H. J.; Herz, L. M. Charge-carrier mobility and localization in semiconducting Cu_2AgBiI_6 for photovoltaic applications. ***ACS Energy Lett.*** **2021**, *6* (5), 1729-1739.

(4) Wehrenfennig, C.; Eperon, G. E.; Johnston, M. B.; Snaith, H. J.; Herz, L. M. High Charge carrier mobilities and lifetimes in organolead trihalide perovskites, ***Adv. Mater.*** **2014**, *26* (10), 1584-1589.